Conductance and gating effects at sputtered oxide interfaces

Yin, C.

6

Tunable magnetic interactions in $LaAlO_3/SrTiO_3$ heterostructures by ionic liquid gating

The gating effect achieved by an ionic liquid and its electric double layer allows for charge transfer which can be an order of magnitude larger than with conventional dielectrics. However, the large charged ions also causes inevitable Coulomb scattering in the conducting channel formed at the interface, which can limit the carrier mobility enhancement. In this Chapter, we study the effect of the $LaAlO_3$ thickness on the transport properties in $LaAlO_3/SrTiO_3$ heterostructures by ionic liquid gating. We find that the transport properties of the $LaAlO_3/SrTiO_3$ interface are dominated by the intrinsic interactions rather than the $LaAlO_3$ thickness and possible effects from the ions in the liquid. We observe a Kondo effect, which is enhanced while increasing the gate voltage. We also observe a gate-tunable and temperature-dependent anomalous Hall effect, which always emerges near the Kondo temperature. Our experiments pave the way to manipulate the various magnetic interactions in $LaAlO_3/SrTiO_3$ heterostructures.

An adapted version of this Chapter has been submitted for publication in a peer-reviewed journal as C. Yin, K. Prateek, W. Gelling, and J. Aarts, *Tunable magnetic interactions in $LaAlO_3/SrTiO_3$ heterostructures by ionic liquid gating*, arXiv preprint [178].

6.1. Introduction

The two-dimensional electron system (2DES) at the interface between $LaAlO_3$ and $SrTiO_3$ [9] has been the focus of intensive studies due to its intriguing properties, such as superconductivity [6], signatures of magnetism [10, 11, 15] and even their coexistence [7, 12]. The 2DES properties can also be modulated by electrostatic gating. Pioneering works have been performed in the back-gate configuration, where the dielectric insulator is the $SrTiO_3$ substrate. Novel gate-tunable effects, such as insulator to metal transition [26], insulator to superconductor transition [71] and Rashba spin-orbit coupling [18, 72] have been reported. However, in this configuration high voltages of tens to hundreds of volts are required to achieve a sizable gating effect. Moreover, the high voltages also induce unavoidable modifications to the defect landscape in the $SrTiO_3$ substrate as discussed in Chapter 4. The top-gate geometry works in a similar way as the back-gate counterpart, but the insulating dielectric is the $LaAlO_3$ overlayer. Compared with back-gating, the big advantage of top-gating is that it requires very low voltages to achieve sizeable gating effects. However, the device fabrication process is very complicated which is due to the requirement of multiple aligned lithography steps [91].

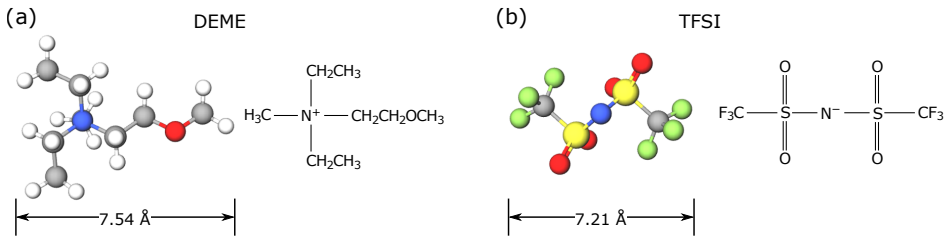

Figure 6.1: Molecular structures and molecular formulas of (a) positively charged DEME and (b) negatively charged TFSI. Average diameters of DEME and TFSI are 7.54 Å and 7.21 Å, respectively [179].

Electric double layer transistors (EDLTs) of the top-gate configuration provide an alternative approach. In recent years, EDLTs have generated considerable research interest due to the capability of inducing high carrier densities in materials. EDLTs have been used for inducing superconductivity in $SrTiO_3$ [94] and $KTaO_3$ [95] as well as for tuning transport properties in $LaAlO_3/SrTiO_3$ heterostructures [70, 99, 100]. EDLTs use ionic liquids (ILs) as gate dielectrics, in which the size of the ions is usually larger than the lattice parameter of perovskite oxides. For instance, the average diameter of the ions in a widely used IL, called DEME-TFSI[1] as shown in Fig. 6.1, is about 7 Å [179]. When the electrolyte touches the channel, the long-range Coulomb potentials created by the ions

[1] Molecular formula is N,N-diethyl-N-methyl-N-(2-methoxyethyl)-ammonium bis-trifluoromethylsulfonyl)-imide

will cause inevitable scattering of the conduction electrons and therefore limit the mobility enhancement, as was shown for experiments on BN-encapsulated graphene [180]. In a similar fashion, Gallagher *et al.* [181] have recently reported a ten-fold improvement of the carrier mobility in $SrTiO_3$ single crystals by covering the channel with a thin BN flake.

In $LaAlO_3/SrTiO_3$ heterostructures, the $LaAlO_3$ film is a natural protection for the channel. However, one would expect that there is a trade-off between obtaining high carrier densities, which requires thin $LaAlO_3$ layers, and achieving high mobilities, which requires thick $LaAlO_3$ layers. In this Chapter, we study the effect of the $LaAlO_3$ film thickness on the transport properties of three $LaAlO_3/SrTiO_3$ EDLTs. We obtain the largest tunability in a device with about 4 unit cells (uc) of $LaAlO_3$. We observe a gate-tunable Kondo effect in all the devices. More interestingly, we also observe a temperature-dependent nonlinearity of the Hall resistance, which is always accompanied by the emergence of a Kondo effect. We attribute this anomaly to an anomalous Hall effect. Our results imply that the transport properties of $LaAlO_3/SrTiO_3$ EDLTs are mainly governed by the intrinsic interactions, while the $LaAlO_3$ thickness has a minor effect.

6.2. Experiments

A schematic of the EDLT device is shown in Fig. 6.2(a). The Hall bar pattern was fabricated by photolithography as discussed in Chapter 2. The length between two voltage probes is 500 µm, and the Hall bar width is 50 µm. It is well known that the critical thickness of $LaAlO_3$ which gives rise to a conducting interface is 4 uc [26]. We fabricated three devices with difference thickness of $LaAlO_3$ layer by using the calibrated growth rate of 4.3 Å/min to estimate the thickness. Growth times were 3.5, 7.0 and 10.5 min, respectively, yielding the devices with thicknesses of 1.5, 3.0 and 4.5 nm, which we refer to as 4uc, 8uc and 12uc. The $LaAlO_3$ films were deposited at 800 °C and an Ar pressure of 0.04 mbar by 90° off-axis sputtering. Fig. 6.2(b)-(d) depict the AFM images of the $LaAlO_3$ surface of the three devices. After sample fabrication, a droplet of IL, DEME-TFSI (IOLITEC) was applied onto the device surface covering the gate electrode and the channel.

The magnetotransport measurements were performed in the PPMS at temperatures down to 3 K. As shown in Fig. 6.2(a), a Keithley 6221 current source was used to apply a direct current (I_{DC} = 1.0 µA). Two Keithley 2182A nanovoltmeters were used to measure the longitudinal (V_{xx}) and transverse voltages (V_{xy}). The gate voltage (V_G) was applied by a Keithley 2400 source meter. The freezing point of DEME-TFSI is ~180 K. As a general procedure, we applied V_G at 210 K and then waited for ~15 min for the IL to equilibrate. The measurements were started at 150 K and the leakage current was less than 1.0 nA during the measurements.

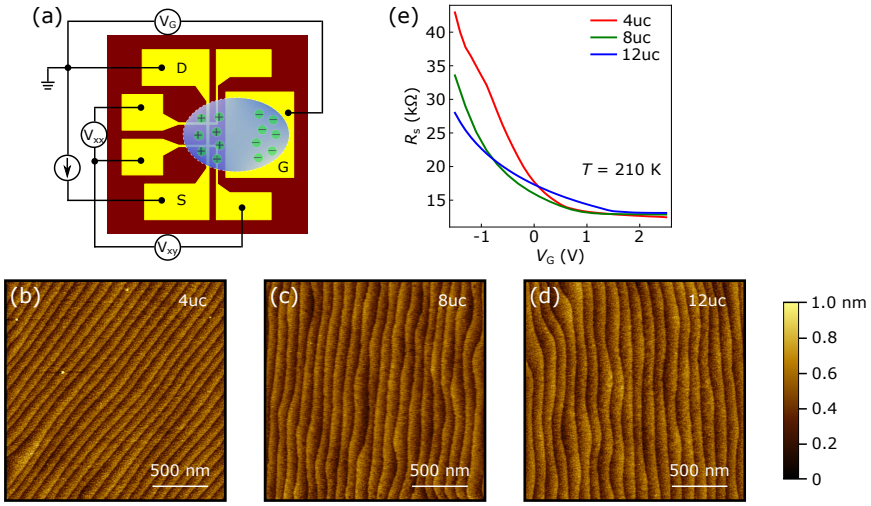

Figure 6.2: (a) Schematic of the EDLT device. Source and drain are labeled as "S" and "D". The longitudinal (V_{xx}) and transverse voltages (V_{xy}) are measured simultaneously. Gate voltage (V_G) is applied between the gate electrode ("G") and the drain. (b)-(d) AFM images of the $LaAlO_3$ surface taken at the Hall bar channel of devices (b) 4uc, (c) 8uc and (d) 12uc. (e) Sheet resistance (R_s) as a function of V_G at 210 K of the three devices with different thickness of the $LaAlO_3$ layer as indicated.

Fig. 6.2(e) shows the sheet resistance (R_s) as a function of V_G at 210 K of the three devices. As expected, the gate tuning effect on R_s decreases as the $LaAlO_3$ thickness increases. Above $V_G = 1.5$ V, R_s almost saturates in all of the devices. We find that the gate voltage sweeps are nicely reproducible, which allows us to exclude any possible electrochemical reaction occurring on $LaAlO_3$ surface [94]. The forward and backward sweeps are also reversible, indicating that no electron trapping is induced in the top-gate configuration.

6.3. Tuning of Kondo effect

First, we present the temperature dependence of R_s measured under various values of V_G. Fig. 6.3(a) shows the data of device 4uc. At $V_G = 0$ V, R_s first decreases from 150 K to 10 K and then remains unchanged. In the negative voltage regime, R_s decreases monotonously to 3 K, but in the positive voltage regime, R_s first reaches a minimum at ~ 30 K and then increases as temperature decreases to 3 K. As shown in Fig. 6.3(b) and 6.3(c), the resistance minimum is always present for devices 8uc and 12uc. For a better view, the resistance relative to its value at 3 K, $R_s(T) - R_s(3\,\mathrm{K})$, is plotted in Fig. 6.3(d)-(f). In earlier reports, this resistance upturn has been attributed to either a weak localization (WL) effect [71, 182] or a Kondo effect [70, 183]. We observed positive magnetoresistance

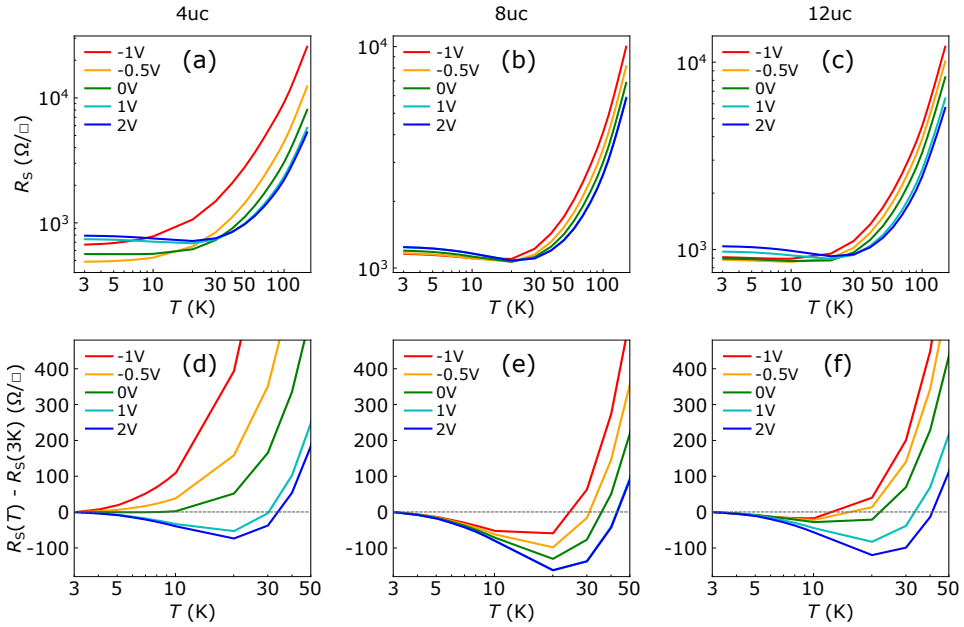

Figure 6.3: (a)-(c) Sheet resistance (R_s) as a function of temperature at various gate voltages of devices (a) 4uc, (b) 8uc and (c) 12uc. (d)-(f) Corresponding R_s relative to its value at 3 K, $R_s(T)-R_s(3\,\mathrm{K})$ of the three devices.

(MR) with sharp cusps in low magnetic fields at 3 K in all of the devices as shown in the supplemental material (Fig. 6.8, 6.9 and 6.11). The sharp cusps in low magnetic fields are characteristic features of a weak antilocalization (WAL) effect (see also Chapter 5) [72, 171] and allows us to exclude the WL effect.

In a metallic system where itinerant electrons couple antiferromagnetically with localized moments, spin-flip scattering gives rise to a resistance minimum, which is known as the Kondo effect [184]. The Kondo effect is characterized by a Kondo temperature, T_K. For $T < T_K$, the resistance increases logarithmically and eventually saturates at low temperatures. The $R_s(T)$ can be described by a simple formula [183]

$$R(T) = R_0 + aT^2 + bT^5 + R_K(T/T_K), \tag{6.1}$$

where R_0 is the residual resistance, and the T^2 and T^5 terms represent the temperature-dependent electron-electron and electron-phonon interactions, respectively. $R_K(T/T_K)$ is a universal resistivity function with the empirical form

$$R_K(T/T_K) = R_K(0\,\mathrm{K})\left(\frac{1}{1+(2^{1/s}-1)(T/T_K)^2}\right)^s, \tag{6.2}$$

where $R_K(0\,\mathrm{K})$ is the Kondo resistance at zero temperature and $s = 0.225$. Fig. 6.4(a)

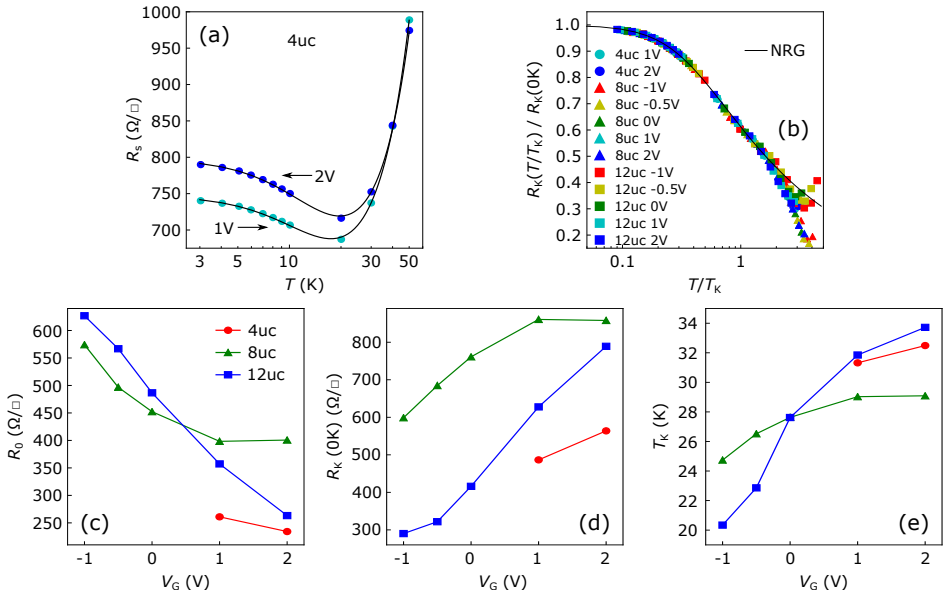

Figure 6.4: (a) R_s minimum observed from 3 to 50 K of device 4uc at 1 V and 2 V. The black lines are the Kondo effect fits using Eqs. (6.1) and (6.2). (b) Normalized Kondo resistance ($R_K(T/T_K)/R_K(0K)$) versus reduced temperature (T/T_K) curves of the three devices collapse into a single black line, which is obtained from the numerical renormalization group (NRG) method. (c)-(e) Extracted Kondo parameters, (d) the residual resistance (R_0), (e) the Kondo resistance at zero temperature ($R_K(0K)$) and (f) the Kondo temperature (T_K), as a function of V_G of the three devices.

shows the fitting results of device 4uc at V_G = 1 V and 2 V. The extracted values of R_0, $R_K(0K)$ and T_K as a function of V_G for the three devices are plotted in Fig. 6.4(c)-(e).

Numerical renormalization group (NRG) method normalizes the Kondo contribution to the transport by a universal parameter T/T_K [185]. It is often used as a criterion to verify the Kondo scenario. As shown in Fig. 6.4(b), $R_K(T/T_K)/R_K(0K)$ as a function of T/T_K measured under various V_Gs of the three devices all collapse into a single curve, which confirms that the Kondo effect is the origin of the observed resistance minimum. As can be seen from Fig. 6.4(d)-(e) in particular, $R_K(0K)$ and T_K are a function of the gate voltage. Such a gate-tunable Kondo effect has been previously observed in undoped $SrTiO_3$ single crystals [183], $LaAlO_3/SrTiO_3$ [70] and γ-$Al_2O_3/SrTiO_3$ [186] EDLTs, and is consistent with our results. It is noteworthy to mention that this Kondo effect is caused by the interactions between itinerant electrons and localized electrons [183] rather than with conventional magnetic impurities, such as iron. In the presence of magnetic impurities, one would expect to observe a stronger Kondo effect at a lower carrier density, while here the gate voltage increases the carrier density.

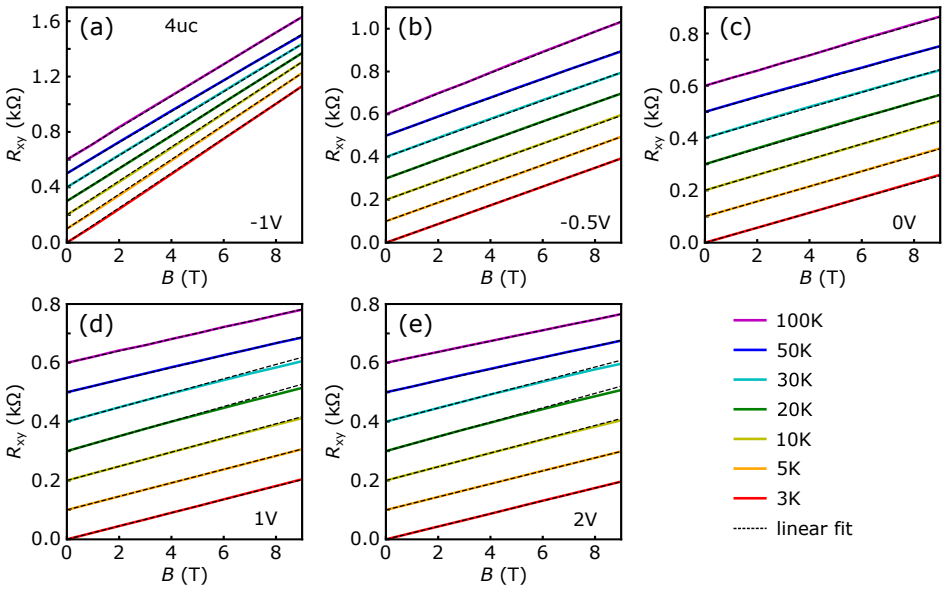

Figure 6.5: Hall resistance (R_{xy}) of device 4uc measured at various temperatures and under various gate voltages. The curves are separated by an offset of 100 Ω for clarity. The dotted lines are linear fits to $R_{xy}(B)$.

6.4. Tuning of anomalous Hall effect

Next, we present the temperature-dependent nonlinearity of the Hall resistance (R_{xy}) measured under various V_Gs. Fig. 6.5 shows the data of device 4uc. The $R_{xy}(B)$ curves are separated by an offset of 100 Ω for clarity and the dotted lines are their linear fits. For the cases of $V_G = -1$ V, -0.5 V and 0 V as shown in Fig. 6.5(a)-(c), the $R_{xy}(B)$ curves are linear at all temperatures. For the other cases as shown in Fig. 6.5(d)-(e), the $R_{xy}(B)$ curves are linear at high temperatures (above 50 K) and low temperatures (below 10 K), but nonlinear at intermediate temperatures. For devices 8uc and 12uc, the nonlinear $R_{xy}(B)$ curves are observed at all V_Gs (see supplemental material, Fig. 6.10 and 6.12). We find that the emergence of nonlinear $R_{xy}(B)$ is always accompanied by the observation of the Kondo effect.

One possibility for a nonlinear Hall effect is two-band transport [63, 89]. The band structure of the $LaAlO_3/SrTiO_3$ interface is formed by the Ti t_{2g} orbitals. For $LaAlO_3$ films grown on $SrTiO_3$ (001) substrates, the d_{xy} band stays below the $d_{xz,yz}$ bands in energy, as shown in Fig. 5.1 [61, 89, 124]. In the one-band regime, only the d_{xy} band is populated. The carrier density (n_s) and mobility (μ) can be determined by $n_s = B/eR_{xy}$ and $\mu = R_{xy}/BR_s(B=0)$, where e is the electron charge. Tuning the Fermi level to above the bottom of the $d_{xz,yz}$ bands triggers a Lifshitz transition, resulting in a nonlinear $R_{xy}(B)$.

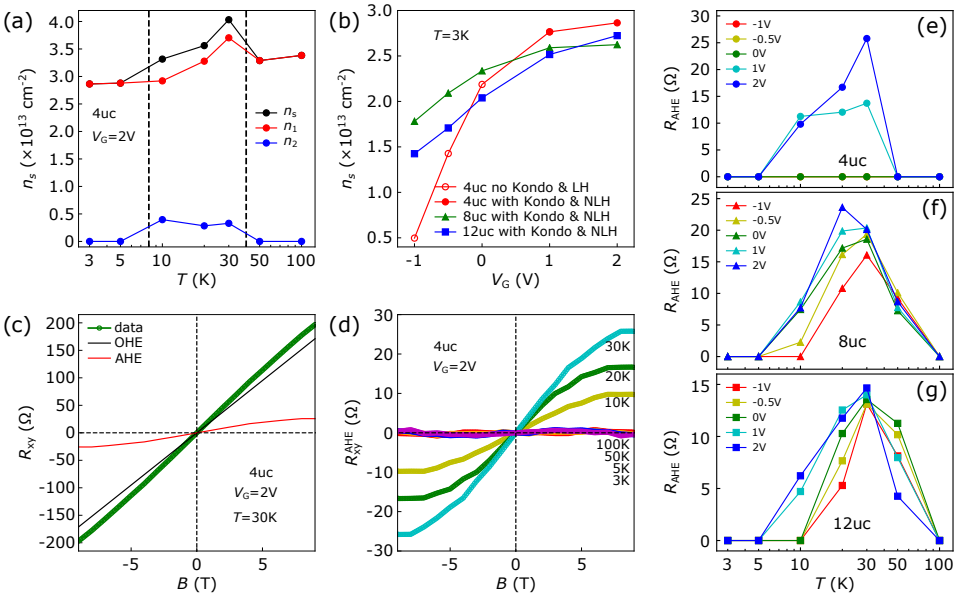

Figure 6.6: (a) Temperature dependence of the carrier density (n_s) of device 4uc at V_G = 2 V. The values are extracted by fitting the magnetotransport data with a two-band model. n_1 and n_2 represent the carrier densities of different conduction channels and their sum is n_s. (b) n_s as a function of V_G of the three devices at 3 K. Open symbols represent no observation of Kondo effect and linear Hall (LH) effect at intermediate temperatures and solid symbols represent the observation of Kondo effect and nonlinear Hall (NLH) effect at intermediate temperatures. (c) An example for the determination of OHE and AHE terms from R_{xy} measured on device 4uc at 30 K and V_G = 2 V. (d) Deduced AHE as a function of magnetic field at various temperatures of device 4uc at V_G = 2 V. (e)-(g) Anomalous Hall resistance (R_{AHE}) as a function of temperature at various V_Gs of devices (e) 4uc (f) 8uc and (g) 12uc.

In the two-band regime, the carrier densities and mobilities can be extracted by fitting the magnetotransport data with a two-band model [128]

$$R_s = \frac{1}{e}\cdot\frac{\frac{n_1\mu_1}{1+(\mu_1 B)^2}+\frac{n_2\mu_2}{1+(\mu_2 B)^2}}{\left(\frac{n_1\mu_1}{1+(\mu_1 B)^2}+\frac{n_2\mu_2}{1+(\mu_2 B)^2}\right)^2+\left(\frac{n_1\mu_1^2 B}{1+(\mu_1 B)^2}+\frac{n_2\mu_2^2 B}{1+(\mu_2 B)^2}\right)^2}, \tag{6.3}$$

$$R_{xy} = \frac{B}{e}\frac{\frac{n_1\mu_1^2}{1+\mu_1^2B^2}+\frac{n_2\mu_2^2}{1+\mu_2^2B^2}}{(\frac{n_1\mu_1}{1+\mu_1^2B^2}+\frac{n_2\mu_2}{1+\mu_2^2B^2})^2+(\frac{n_1\mu_1^2 B}{1+\mu_1^2B^2}+\frac{n_2\mu_2^2 B}{1+\mu_2^2B^2})^2}, \tag{6.4}$$

where n_1 and n_2 are the carrier densities of the first and second conduction bands, respectively, and μ_1 and μ_2 are the corresponding mobilities. For a reliable convergence n_2 and μ_2 are set to 0 in the one-band transport regime. We note that n_1 has a d_{xy} character and n_2 has a $d_{xz,yz}$ character.

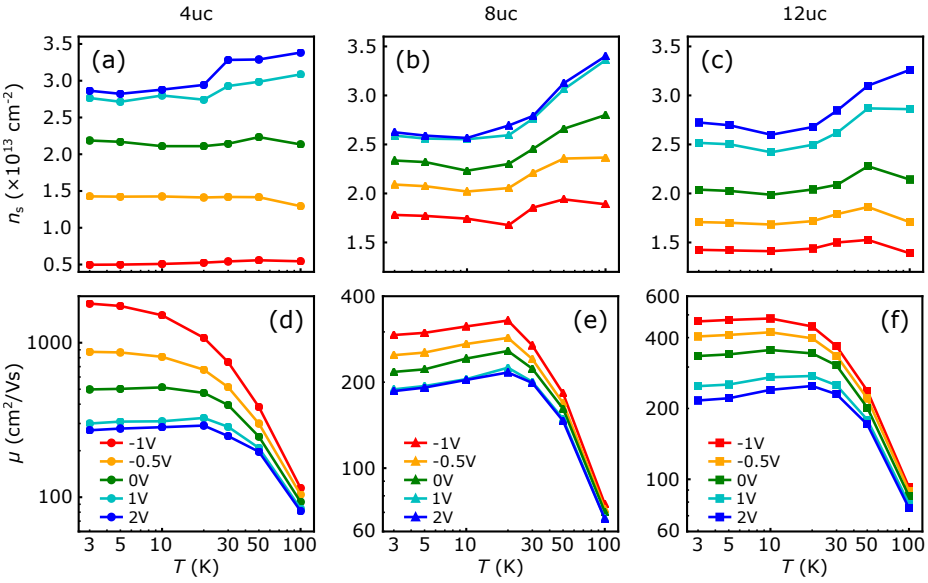

Figure 6.7: Temperature dependence of (a)-(c) carrier density (n_s) and (d)-(f) mobility (μ) of the three devices measured under various gate voltages. The values are obtained by fitting R_{xy}^{OHE}.

Fig. 6.6(a) plots the carrier density as a function of temperature of device 4uc at $V_G = 2$ V as an example. It can be seen that the total carrier density ($n_s = n_1 + n_2$) is 2.86×10^{13} cm^{-2} at 3 K and increases to 4.03×10^{13} cm^{-2} at 30 K, corresponding to an increase of ~ 41 %. In earlier reports, such a nonlinear Hall effect at intermediate temperatures has been only reported in a 26 uc $LaAlO_3/SrTiO_3$ sample [187], where the occupation of the $d_{xz,yz}$ bands has been attributed to thermally excited electrons. However, we argue that two-band conduction cannot serve as a convincing explanation for our results. First, when the 2DES enters the nonlinear regime, we obtain a large increase of n_s, ranging from 22 % to 41 %, in our three devices at various V_Gs. But in Ref. [187], the increase is only ~ 3 %, which is much less than our case. Second, for the cases of device 4uc at $V_G = -1$ V, -0.5 V and 0 V, we find that n_s remains almost constant at all temperatures. If thermal excitation indeed gives rise to additional electrons, one would expect to observe an increase of n_s under all V_Gs. Third, in earlier reports, the critical carrier density (n_L) window for Lifshitz transition is $1.7-2.9 \times 10^{13}$ cm^{-2} [63, 89]. We found a similar value in Chapter 4. Within our measurement limit, we observe linear $R_{xy}(B)$ at 3 K in all of the devices. Fig. 6.6(b) shows the extracted n_s(3 K) as a function of V_G. The threshold carrier density for the emergence of Kondo effect differs among devices, but the overall trend is the same. Most of the values are in the n_L window, which indicates that a higher magnetic field is required to reliably analyze the transport regime and find

the expected two-band behavior. Taken together, the data at 3 K appear to preclude a two-band explanation for the nonlinear Hall effect at intermediate temperatures.

An alternative possibility for the nonlinear Hall effect is the anomalous Hall effect (AHE), which occurs in solids with ferromagnetic order [188]. In a system with AHE, R_{xy} consists of the ordinary Hall effect (OHE) term and the AHE term. As shown in Fig. 6.6(c) for the 4uc device at 30 K, the OHE term, R_{xy}^{OHE}, can be obtained from a linear fit to the high field limit of R_{xy}. Subtracting R_{xy}^{OHE} from R_{xy} will give the AHE term, R_{xy}^{AHE} [189]. Fig. 6.6(d) shows the R_{xy}^{AHE} contributions obtained at various temperatures for device 4uc at $V_G = 2$ V. Similar to common observations in the $LaAlO_3/SrTiO_3$ system, the R_{xy}^{AHE} curves show no hysteresis. Gunkel *et al.* [114] have proposed a phenomenological Langevin-type function in the spirit of the polarization of magnetic moments to describe R_{xy}^{AHE}. However, we could not obtain a satisfactory fit due to the lack of a clear magnetization saturation in the limited magnetic field. Christensen *et al.* [14] have recently reported a non-saturating AHE even up to 15 T. Fig. 6.6(e)-(g) show the anomalous Hall resistance (R_{AHE}) taken from the high field limit of R_{xy}^{AHE}, which increases as V_G is increasing. Similar temperature-dependent AHE effect has been reported in $SrTiO_3$ single crystals [190] and $LaAlO_3/SrTiO_3$:Fe heterostructures [191]. Fig. 6.7(a)-(c) and 6.7(d)-(f) plot the n_s and μ as a function of temperature of the three devices under various V_Gs. The values are obtained by fitting R_{xy}^{OHE} with a one-band model. The largest tunability is obtained from device 4uc.

6.5. Discussion

The Kondo effect originates from antiferromagnetic coupling between itinerant electrons and localized spins [184]. In our $LaAlO_3/SrTiO_3$ system, the Kondo scattering centers are localized and unpaired electrons [183]. The density of these localized electrons increases when increasing V_G. The temperature range in which AHE emerges is closely related to T_K. At low temperatures, $T \ll T_K$, the localized spins are effectively screened by the continuum states of the metal host upon forming coherent many-body singlet states [192]. A rough estimation of the energy scale, $g\mu_B B \approx k_B T_K$ ($g = 2$ is the g factor, μ_B is the Bohr magneton and k_B is the Boltzmann constant), indicates that a magnetic field of several tens of Tesla is required to break down the Kondo screening. Therefore a linear R_{xy} is observed. At high temperatures, $T \gg T_K$, the alignment of localized moments by magnetic field is countered by thermal fluctuations, resulting in a linear R_{xy} as well. At intermediate temperatures, $T \sim T_K$, ferromagnetic interactions between localized spins could give rise to a strong magnetic polarization in a magnetic field, resulting in the anomalous Hall effect. The origin of this non-hysteretic magnetization is still unclear. It appears to be due to the polarization of unpaired spins [80, 193], although spiral

magnetic ordering [194] might also be possible.

6.6. Conclusion

In summary, we have studied the effect of $LaAlO_3$ film thickness on the transport properties of $LaAlO_3/SrTiO_3$ EDLTs, and obtained the largest tunability in terms of carrier density and mobility in the device with 4 uc of $LaAlO_3$. We have shown a gate-tunable Kondo effect which originates from localized electrons. More interestingly, we have also observed a gate-tunable anomalous Hall effect which always emerges near the Kondo temperature. Our results show that the physical properties of $LaAlO_3/SrTiO_3$ EDLTs are dominated by the intrinsic interactions, while the $LaAlO_3$ thickness has a secondary effect. Our experiments provide insights to understand the observed magnetism at the $LaAlO_3/SrTiO_3$ interface and demonstrate a non-trivial tuning of magnetic interactions by ionic liquid gating, paving the way for designing novel electronic devices based on $LaAlO_3/SrTiO_3$ heterostructures.

Supplemental material

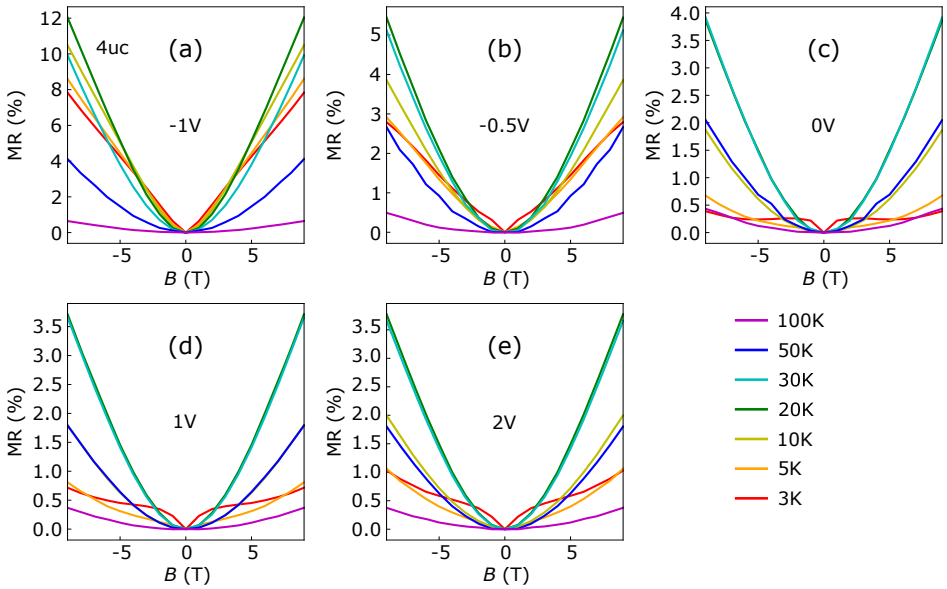

Figure 6.8: Magnetoresistance (MR) of device 4uc measured at various temperatures and under various gate voltages.

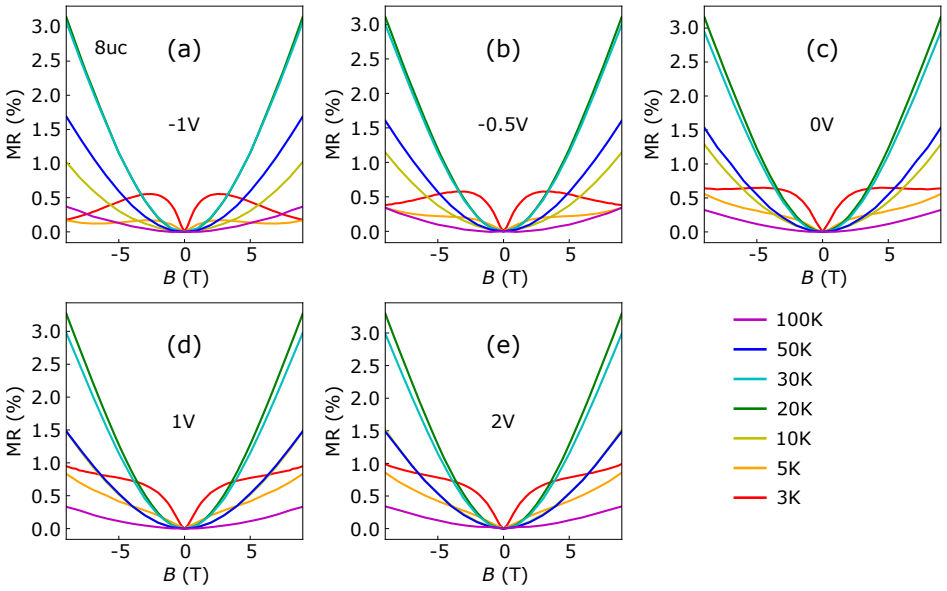

Figure 6.9: Magnetoresistance (MR) of device 8uc measured at various temperatures and under various gate voltages.

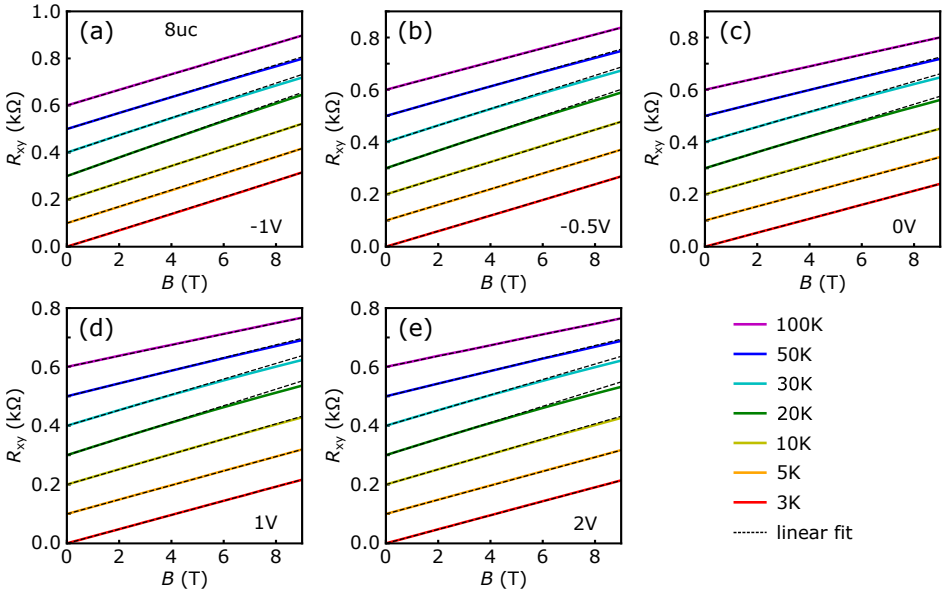

Figure 6.10: Hall resistance (R_{xy}) of device 8uc measured at various temperatures and under various gate voltages. The curves are separated by an offset of 100 Ω for clarity. The dotted lines are linear fits to $R_{xy}(B)$.

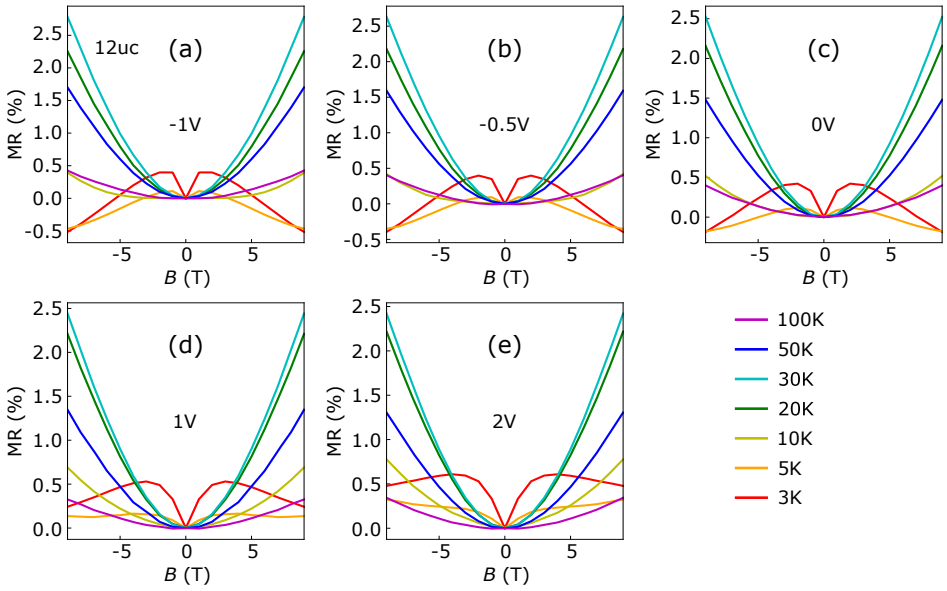

Figure 6.11: Magnetoresistance (MR) of device 12uc measured at various temperatures and under various gate voltages.

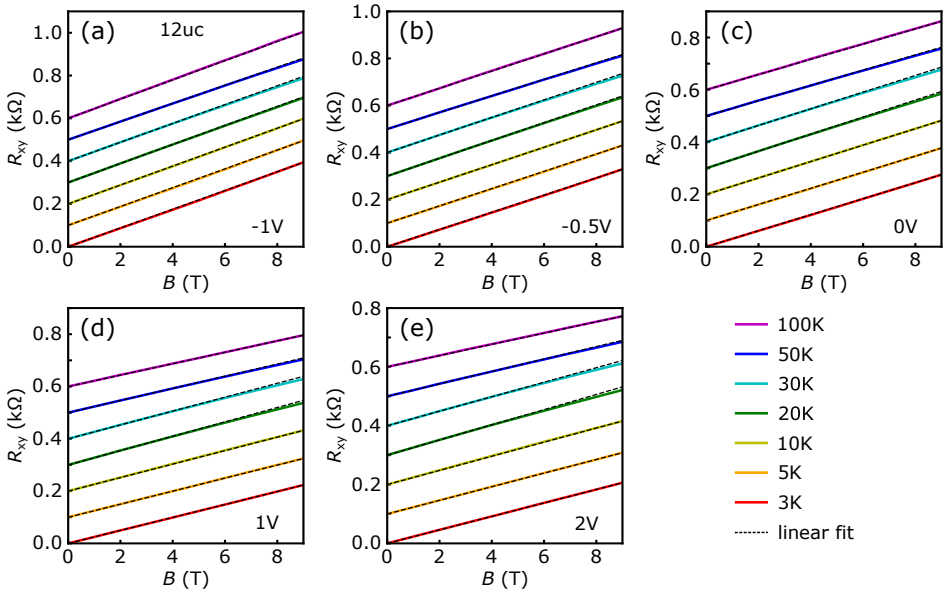

Figure 6.12: Hall resistance (R_{xy}) of device 12uc measured at various temperatures and under various gate voltages. The curves are separated by an offset of 100 Ω for clarity. The dotted lines are linear fits to $R_{xy}(B)$.